Letter

Correlation-induced Fermi surface evolution and topological crystalline superconductivity in $CeRh_2As_2$

Jun Ishizuka [1,2] Kosuke Nogaki [3] Manfred Sigrist [2] and Youichi Yanase [3]
[1]*Faculty of Engineering, Niigata University, Ikarashi, Niigata 950-2181, Japan*
[2]*Institute for Theoretical Physics, ETH Zürich, 8093 Zürich, Switzerland*
[3]*Department of Physics, Graduate School of Science, Kyoto University, Kyoto 606-8502, Japan*

(Received 31 October 2023; revised 2 September 2024; accepted 24 September 2024; published 15 October 2024)

Locally noncentrosymmetric structures in crystals are attracting much attention owing to emergent phenomena associated with the sublattice degree of freedom. The newly discovered heavy fermion superconductor $CeRh_2As_2$ is considered to be an excellent realization of this class. Angle-resolved photoemission spectroscopy experiments recently observed low-energy spectra of electron and hole bands and characteristic Van Hove singularities, stimulating us to explore the electronic correlation effect on the band structure. In this Letter, we theoretically study the electronic state and topological superconductivity from first principles. Owing to the Coulomb repulsion U of Ce $4f$ electrons, the low-energy band structure is modified in accordance with the experimental result. We show that Fermi surfaces change significantly from a complicated three-dimensional structure to a simple two-dimensional one. Fermi surface formulas for one-dimensional $\mathbb{Z}_2$ invariants in class D indicate topological crystalline superconductivity protected by the glide symmetry in a broad region for U. The classification of superconducting gap structure reveals the topologically protected excitation gap and node. Our findings of the correlation-induced evolution of electronic structure provide a basis to clarify the unusual phase diagram of $CeRh_2As_2$ including superconductivity, magnetic order, and quadrupole density wave, and accelerate the search for topological superconductivity in strongly correlated electron systems.

DOI: 10.1103/PhysRevB.110.L140505

I. INTRODUCTION

The locally noncentrosymmetric superconductor $CeRh_2As_2$ stands out because it shows two distinct superconducting phases under magnetic fields directed along the c axis [1]. The upper critical field reaches 14 T at zero temperature, significantly exceeding the Pauli paramagnetic limit in view of the low critical temperature, $T_c \approx 0.35$ K. Rotating the field toward the ab plane quickly suppresses the critical field down to 2 T, and the high-field superconducting phase disappears [2]. This high-field phase is consistently described as a pair-density wave (PDW) with an order parameter switching from a uniform even to a uniform odd-parity pairing state [1–5].

The unusual superconducting phase diagram seems to emerge from strongly correlated electrons. The specific heat coefficient is enhanced as $\gamma \sim 1000$ mJ/mol K^2, indicating strong influence by Ce $4f$ electrons, and superconductivity occurs from the resistivity $\rho \propto \sqrt{T}$, suggesting the quantum criticality [1]. Intriguingly, a nonmagnetic quadrupole density wave above T_c has been proposed based on the resistivity, specific heat, and thermal expansion measurements [1,6–8]. The appearance of antiferromagnetic order within the superconducting phase has also been suggested by nuclear quadrupole and magnetic resonance measurements [5,9,10], in which magnetic moments are thought to break global inversion symmetry in the system.

Theoretical studies of $CeRh_2As_2$ have provided further insight into superconductivity and electronic states [11–21]. The crystal structure has an inversion center between two Ce atoms but not on the Ce atom. We refer to such a property as local inversion symmetry breaking. Due to the lack of inversion symmetry on the Ce atom, staggered antisymmetric spin-orbit coupling (ASOC) plays a central role. The impact of such staggered ASOC depends on the ASOC and the interlayer hopping ratio, and can be enhanced if the latter is weak [3,22]. Indeed, Rh_2As_2 block layers considerably reduce interlayer hopping between the Ce atoms, and the nonsymmorphic crystal symmetry exactly prohibits this hopping at the Brillouin zone boundary [16,22]. As a consequence, unusual H-T phase diagrams involving even and odd-parity superconducting phases are highly expected [12,14,16,17].

The low-energy electronic structure near the Fermi level is crucial to verify these scenarios. First-principles calculations show that the low-energy states are well described by the Ce $4f$ bands hybridizing with Rh $4d$ bands [6,13,15,16], consistent with the heavy fermion behavior observed in experiments. However, the optical conductivity measured in the experiment quantitatively deviates from the simple hybridization picture and suggests the importance of the correlation effects [23]. Renormalized band structure calculations have been conducted to gain insight into the electronic state [6,16]. The hole and electron Fermi surfaces (FSs) are elliptical and cylindrical in the renormalized band calculation, whereas they have a complex three-dimensional (3D) structure in the standard bare band calculation. It should be noted that the magnetic field separating the low- and high-field superconducting phases H^* reaches $H^*/T_c \sim 10$ in $CeRh_2As_2$ [1],

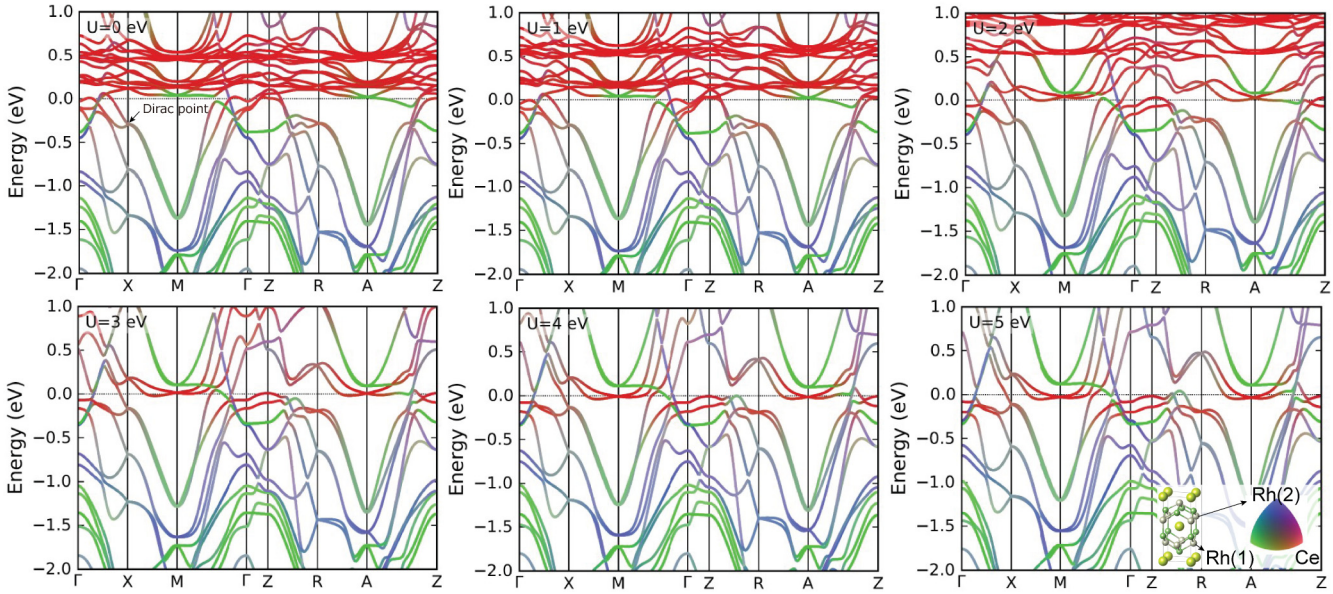

FIG. 1. Band structure along the high symmetry lines by the DFT + U calculation with various values of U. The red, green, and blue colors represent the weight of atoms for Ce, Rh(1), and Rh(2), respectively.

which is consistent rather with the fluctuation exchange analysis ∼15 [17] than with the mean-field value ∼2 [3]. This fact also implies the presence of strong correlation effects in $CeRh_2As_2$.

Studies of $CeRh_2As_2$ may impact research on topological superconductivity because designing topological materials is a central issue in modern condensed matter physics. Thanks to the recent topological classification theory, several setups for topological superconductivity have been identified [24–29]. The concept of topological crystalline superconductivity (TCSC), in which the nontrivial topology is protected by crystalline symmetry, has opened up a vast area of research [30–51]. For example, it has been proposed that UPt_3 [43], UCoGe under pressure [44], and the PDW state in $CeRh_2As_2$ [13] can be topological crystalline superconductors protected by the nonsymmorphic glide symmetry. For $CeRh_2As_2$, topological $\mathbb{Z}_2$ invariants defined in the glide invariant $\boldsymbol{k}$ space can be calculated by counting the number of FSs on the high symmetry Γ-M and Z-A lines. Indeed, the previous study concluded the TCSC from a first-principles calculation [13]. However, it is widely known that the first-principles band calculations may be insufficient to predict FSs of f-electron systems because of the strong correlation, e.g., $CeCoIn_5$ [52,53], $CeIrIn_5$ [54], $CeCu_2Si_2$ [55], and UTe_2 [56,57]. Therefore, clarifying the topological nature of $CeRh_2As_2$ with the strong correlation among the f electrons is highly desired.

In this work, we investigate the electronic state in paramagnetic $CeRh_2As_2$ with the electronic correlation effects by the density functional theory plus Hubbard U (DFT + U) calculations. We show the dimensional crossover of the FSs from 3D to two dimension (2D) due to the correlation effects. The band dispersion for intermediate U is in good agreement with the recent angle-resolved photoemission spectroscopy (ARPES) experiment [58,59]. Linking the FS topology to the FS formula of topological invariants, we show that the TCSC is stable in a wide region for the interaction parameter U. In addition, the superconducting gap structures are predicted in terms of symmetry and topology. Combining the results, the low-energy excitation in the bulk and the Majorana states on the surface are predicted for all the odd-parity superconducting states.

II. RESULT

A. Band calculations

The atom-resolved band structures by the DFT + U method are summarized in Fig. 1. Details of our band calculation are given in the Supplemental Material [60]. The result for $U = 0$ eV is in good agreement with the previous reports [13,15]. As expected with the usual DFT + U calculation, introducing U lifts some empty Ce $4f$ bands. The low-energy band dispersion on the Γ-X-M-Γ line is well fitted by the ARPES data [58] as shown later. We observe two remarkable features. First, a Dirac point at the X point near -0.3 eV is shifted up toward the Fermi level (~ -0.13 eV for $U = 4$ eV), qualitatively consistent with the recent ARPES measurement, although the ARPES observed it slightly closer to the Fermi level $\sim -75 \pm 60$ meV. The electron bands are fourfold degenerate at the X point because the nonsymmorphic space group symmetry $P4/nmm$ of $CeRh_2As_2$ protects the degeneracy and stabilizes the Dirac electrons [58]. As the Dirac point approaches the Fermi level, a hybridization between Rh and Ce atoms becomes noticeable, resulting in a Van Hove singularity hybridizing with $4f$ electrons close to the Fermi level, consistent with Ref. [58]. Second, electron pockets constructed by the $4f$ electron bands appear around the M and A points for $U \geqslant 1$ eV, involving a change of orbital characters from Rh(1) to Ce. Owing to the flat band properties, both the Van Hove singularity and heavy electron bands may play a significant role for magnetic order, quadrupole order, and superconductivity.

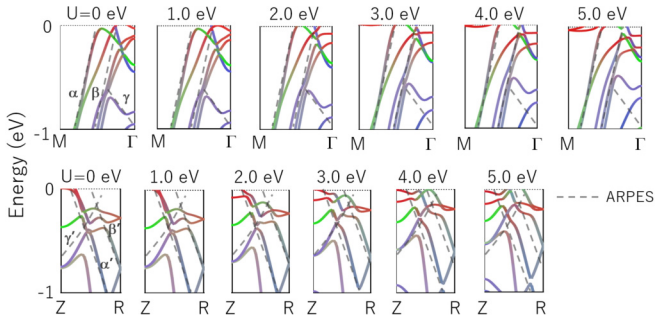

FIG. 2. Band structure by the DFT + U calculation along the M-Γ and Z-R lines. Dashed lines are extracted from the ARPES experiment [58].

Figure 2 compares the DFT + U band structure with the ARPES data along the M-Γ and Z-R lines. ARPES has observed $\alpha(\alpha')$, $\beta(\beta')$, and $\gamma(\gamma')$ branches. The DFT + U results actually capture these branches. Importantly, the $4f$ orbital character is dominant near the Fermi level. Thus, the agreement between the calculation and experiment is found in not only Rh(1) and Rh(2) components but also Ce components, implying the accuracy of the DFT + U approximation. However, we can see some deviations in β' and γ', which do not cross the Fermi level for $U \leqslant 3$ eV. Further experimental and theoretical studies are desired for comparison, e.g., considering the self-energy correction from the localized f electrons by DFT + DMFT. This is beyond the scope of this paper, and we left it for further study. For experiments, accurate observation of the bands close to the Fermi level is desirable.

Figures 3 and 4 show the obtained four FSs, namely, the hole-FS1(2) and electron-FS1(2), in addition to the merged

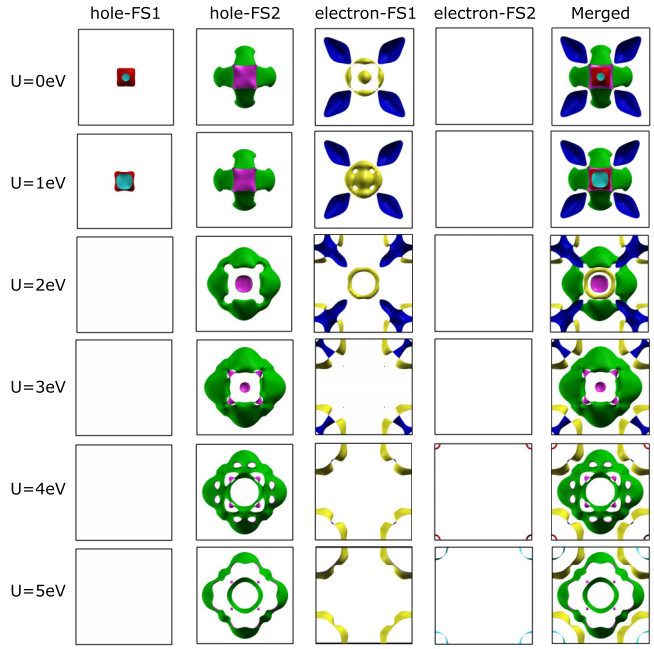

FIG. 3. FSs from the top view by the DFT + U calculation with various values of U.

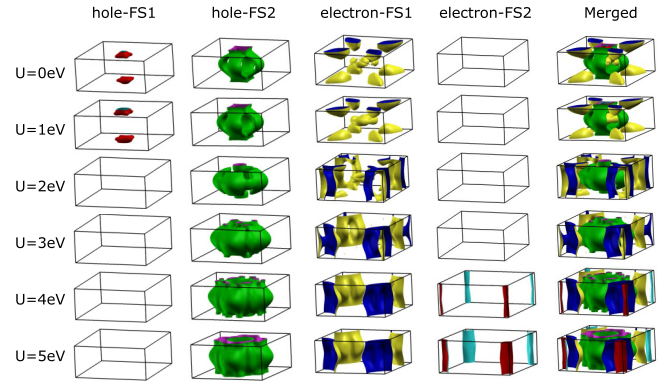

FIG. 4. Evolution of FSs by the DFT + U calculation with increasing the interaction parameter U.

FSs. While the hole-FS1 disappears, the electron-FS2 appears by introducing U. With increasing U, the shape of hole-FS2 and electron-FS1 changes from a 3D shape to a quasi-2D one (see Fig. 3). Here we refer to the 3D (2D) nature of the FSs by their topology, whether they are closed (open) along the k_z direction. The emergence of the 2D nature upon increasing the electron correlation is understood from the crystal structure and the evolution of the c-f hybridization between different layers. The DFT + U result for $U = 3$ eV is partly consistent with the renormalized band calculations [6,16]: (i) the presence of the cylindrical hole-FS2 along the Γ-Z line with a bulge in the basal plane $k_z = 0$ and (ii) the cylindrical electron-FS1 at the zone boundary. However, a Γ-centered closed surface [6,16] is absent in the present calculation. It has been pointed out that the electron-FS1 accounts for 80% of the total density of states and may play a central role in stabilizing the superconducting state [16]. It is also intriguing that we observe disconnected electron and hole pockets with a 2D nature. This is similar to iron-based superconductors, which share the same space group symmetry. In the iron-based superconductors, several electric quadrupole orders have been observed, and fully gapped s-wave superconductivity emerges due to the electric quadrupole and antiferromagnetic spin fluctuations [61–66]. Thus, the evolution of electronic structure due to the electron correlation may be essential for the superconductivity, and conversely, a future experimental study of gap structure will give an insight into the electronic structure. The evolution of FSs as a function of U leads to various topological Lifshitz transitions, which are crucially important for topological superconductivity as we discuss below.

B. Topological crystalline superconductivity

Here, we discuss topological properties of superconductivity in $CeRh_2As_2$. First, we review the FS formulas for the topological invariants obtained in Ref. [13]. We assume odd-parity superconductivity as ensured by the gap function of the PDW state [3,4]. We also assume that the time-reversal symmetry is broken in the superconducting phase because the PDW state is found in $CeRh_2As_2$ under the magnetic field parallel to the c axis [1]. In this magnetic field, the unitary part of the point group is C_{4h}, and the superconducting order parameter is classified into A_u, B_u, and E_u irreducible

TABLE I. $\mathbb{Z}_2$ topological invariants, $\nu_0^{\mathfrak{g}^+}$, $\nu_0^{\mathfrak{g}^-}$, $\nu_\pi^{\mathfrak{g}^+}$, $\nu_\pi^{\mathfrak{g}^-}$, and Chern numbers C_0 and C_π of $CeRh_2As_2$ in the PDW state for various values of U. We assume that the occupation numbers at the Γ_1 and Γ_2 points are unchanged by the magnetic field.

	$(\nu_0^{\mathfrak{g}^+}, \nu_0^{\mathfrak{g}^-}, C_0)$	$(\nu_\pi^{\mathfrak{g}^+}, \nu_\pi^{\mathfrak{g}^-}, C_\pi)$	Weyl SC
$U = 0$ eV	(1, 1, even)	(0, 0, even)	×
$U = 1$ eV	(1, 1, even)	(0, 0, even)	×
$U = 2$ eV	(0, 0, even)	(1, 1, even)	×
$U = 3$ eV	(0, 0, even)	(1, 1, even)	×
$U = 4$ eV	(0, 0, even)	(0, 0, even)	×
$U = 5$ eV	(0, 0, even)	(0, 0, even)	×

representations (IRs). The magnetic space group is represented by $P4/nm'm'$ (No. 129.417), and importantly, the glide symmetry $G = \{\sigma_z|\boldsymbol{a}/2 + \boldsymbol{b}/2\}$ is preserved in this magnetic field. Hereafter, we focus on the glide-invariant planes $k_z = 0, \pi$ and glide-odd superconductivity, namely, the A_u and B_u states corresponding to the PDW state. We can prove that (i) the glide operator anticommutes with the particle-hole operator $\{G, \mathcal{C}\} = 0$, and (ii) the glide eigenvalues for the positive and negative sectors, $\mathfrak{g}^\pm = \pm i \exp[-i(k_x + k_y)/2]$, become pure imaginary in the restricted one-dimensional (1D) $\boldsymbol{k}$-space $k_x + k_y = 0$ (Γ-M and Z-A lines). From (i) and (ii), the particle-hole symmetry is closed in each glide sector. Thus, each glide sector on these lines is classified into 1D superconductors in class D. Therefore, the corresponding topological invariants are given by the 1D $\mathbb{Z}_2$ numbers:

$$\nu_{k_z=0,\pi}^{\mathfrak{g}^\pm} = \frac{1}{\pi}\int_{\Gamma_1}^{\Gamma_2} d\,k_i\,\mathcal{A}_i^{\mathfrak{g}^\pm}(\boldsymbol{k}) \quad (\mathrm{mod}\ 2), \tag{1}$$

where $\mathcal{A}_i^{\mathfrak{g}^\pm}(\boldsymbol{k})$ is the ith component of the Berry connection of each glide sector. Γ_1 and Γ_2 denote the Γ and M points for $k_z = 0$ and, analogously, the Z and A points for $k_z = \pi$. We can identify whether $\nu_{k_z}^{\mathfrak{g}^\pm}$ is trivial or not from the number of Fermi surfaces [67,68] by the formula

$$\nu_{k_z}^{\mathfrak{g}^\pm} = \#\mathrm{FS}_{\Gamma_1\to\Gamma_2}^{\pm} \quad (\mathrm{mod}\ 2). \tag{2}$$

Next, we combine the FS formula with our DFT+U calculations. We obtain $\nu_{k_z}^{\mathfrak{g}^\pm}$ in Table I from Eq. (2) and the DFT+U results in Figs. 3 and 4. The nontrivial topological invariants $\nu_{k_z}^{\mathfrak{g}^\pm}$ are obtained for $U \leqslant 3$ eV. A topological transition occurs between $U = 1$ and 2 eV accompanied by the Lifshitz transition in the hole-FS1 pocket around the Z point and the electron-FS1 pocket around the Γ point. Thorough the topological transition, the invariants change from $(\nu_0^{\mathfrak{g}^\pm}, \nu_\pi^{\mathfrak{g}^\pm}) = (1, 0)$ to $(0, 1)$. These two topological states predict similar surface Majorana fermions. For a large $U \geqslant 4$ eV, the $\mathbb{Z}_2$ invariants are trivial in Table I.

In Table I, we also show $C_{k_z=0,\pi}$ denoting the Chern number whose parity is related to the two Zak phases γ and γ' on the $k_x + k_y = 0$ and $k_x + k_y = \pi$ lines, respectively: $C_{k_z} = \gamma - \gamma'$ (mod 2). By definition, the Zak phase γ on the $k_x + k_y = 0$ line is given by the sum of $\nu_{k_z}^{\mathfrak{g}^\pm}$. Similar formulas to Eq. (2) are valid for the Zak phase γ' on the $k_x + k_y = \pi$ line and enforce γ' to be zero since the occupation numbers

TABLE II. Same as Table I, but we assume the high magnetic field region. The occupation number at the Z point can change due to the Zeeman splitting because the band can be sufficiently flat at the Fermi level near the Z point. Difference in the Chern numbers at $k_z = 0$ and π indicates Weyl superconductivity. We will not discuss the Weyl superconductivity in the case of $C_{k_z} \in 2\mathbb{Z}$ since the integer part of $C_{k_z}/2$ depends on the detailed properties of the gap function.

High field	$(\nu_0^{\mathfrak{g}^+}, \nu_0^{\mathfrak{g}^-}, C_0)$	$(\nu_\pi^{\mathfrak{g}^+}, \nu_\pi^{\mathfrak{g}^-}, C_\pi)$	Weyl SC
$U = 0$ eV	(1, 1, even)	(1, 0, odd) or (0, 1, odd)	○
$U = 1$ eV	(1, 1, even)	(0, 0, even)	
$U = 2$ eV	(0, 0, even)	(1, 1, even)	
$U = 3$ eV	(0, 0, even)	(1, 1, even)	
$U = 4$ eV	(0, 0, even)	(1, 0, odd) or (0, 1, odd)	○
$U = 5$ eV	(0, 0, even)	(0, 0, even)	

are equivalent between the momenta $(\pi, 0, k_z)$ and $(0, \pi, k_z)$ because of the fourfold rotation symmetry. Thus, we obtain $C_{k_z} = \nu_{k_z}^{\mathfrak{g}^+} + \nu_{k_z}^{\mathfrak{g}^-}$ (mod 2), which is even according to Table I. This is consistent with the fact that the Chern number vanishes in the presence of time-reversal symmetry and our DFT+U calculation is carried out at the zero magnetic field.

Here, we discuss the effect of the Zeeman splitting. The Zeeman field lifts the band degeneracy, and the $\mathbb{Z}_2$ invariants will change their values if the occupation numbers at the Γ_1 and Γ_2 points change. Since the g-factor in $CeRh_2As_2$ has not been determined, we estimate the Zeeman splitting with a value $g = 10$ considering an enhancement due to an electron correlation effect [13]. For $U = 0$ and 4 eV, we observe a shallow band across the Fermi level at the Z point ($\sim$4 meV and -7 meV, respectively). It corresponds to the magnetic fields 7 and 12 T, which are lower than the upper critical field $H_{c2} \sim 14$ T. Therefore, the Lifshitz transition may occur due to the magnetic field, and the Chern number C_π and $\mathbb{Z}_2$ invariants $\nu_\pi^{\mathfrak{g}^\pm}$ may become nontrivial (Table II). For different Chern numbers between $k_z = 0$ and π, the Weyl superconductivity accompanied by the topological surface states is predicted [13,69].

To demonstrate the existence of Majorana states, we calculate $(\bar{1}10)$ surface states by using the *ab initio* Wannier model for $U = 2.0$ eV. As shown in Sec. S3 [60], Majorana states appear consistent with the analysis of topological invariants.

C. Superconducting gap nodes

In this section, we elucidate the gap structure in the high-field superconducting state of $CeRh_2As_2$. We first give an ordinary classification theory on superconducting gap nodes based on the point group symmetry [70]. In the absence of the magnetic field, superconducting order parameters are classified into the IRs of the D_{4h} point group. In the presence of the magnetic field, the unitary part of the point group is reduced to C_{4h}. Thus, we can deduce nodes from the basis function of D_{4h} and the compatibility relation to C_{4h}. The gap function is given by $\hat{\Delta}(\boldsymbol{k}) = (\psi_0(\boldsymbol{k})\hat{\sigma}_0 i\hat{\sigma}_y \otimes \hat{\tau}_z + \boldsymbol{d}(\boldsymbol{k})\cdot\hat{\boldsymbol{\sigma}} i\hat{\sigma}_y \otimes \hat{\tau}_0)$, where σ_μ and τ_μ are Pauli matrices for spin and sublattice space. We ignored the orbital degree of freedom. We limit ourselves to the case in which superconductivity is induced by the intrasublattice Cooper pairs of Ce $4f$ electrons. The

TABLE III. Classification of superconducting gap structures for all odd-parity IRs under the magnetic field parallel to the c axis. Results of the Wigner criteria and orthogonality test, effective Altland-Zirnbauer (EAZ) class, and topological classification [60] on the high symmetry lines (i) $k_x + k_y = 0$ with $k_z = 0$, π and (ii) $k_x = k_y = 0$ (k_z axis) are shown. For case (i), the A_u IR in the C_{2h} point group corresponds to the PDW state expected in $CeRh_2As_2$.

(i) $k_x + k_y = 0$, $k_z = 0$ and π

IR of C_{2h}	$W^{\mathfrak{T}}$	$W^{\mathfrak{C}}$	W^{Γ}	EAZ Class	Classification
A_u	1	−1	1	CI	0
B_u	1	0	0	AI	$\mathbb{Z}$

(ii) $k_x = k_y = 0$ (k_z axis)

IR of C_{4h}	$W^{\mathfrak{T}}$	$W^{\mathfrak{C}}$	W^{Γ}	EAZ Class	Classification
A_u	1	0	0	AI	$\mathbb{Z}$
B_u	1	0	0	AI	$\mathbb{Z}$
E_u^1	1	0	0	AI	$\mathbb{Z}$
E_u^2	1	−1	1	CI	0

corresponding basis functions are

$$\boldsymbol{d}_{A_u}(\boldsymbol{k}) = a_1(k_x\hat{\boldsymbol{x}} + k_y\hat{\boldsymbol{y}}) + a_2k_z\hat{\boldsymbol{z}} + a_3(k_y\hat{\boldsymbol{x}} - k_x\hat{\boldsymbol{y}}), \quad (3)$$

$$\psi_{A_u}(\boldsymbol{k}) = a_4\big[1 + k_xk_y\big(k_x^2 - k_y^2\big)\big], \quad (4)$$

and

$$\boldsymbol{d}_{B_u}(\boldsymbol{k}) = b_1(k_x\hat{\boldsymbol{x}} - k_y\hat{\boldsymbol{y}}) + b_2(k_y\hat{\boldsymbol{x}} + k_x\hat{\boldsymbol{y}}), \quad (5)$$

$$\psi_{B_u}(\boldsymbol{k}) = b_3k_xk_y + b_4\big(k_x^2 - k_y^2\big). \quad (6)$$

Considering the basis function, we observe that the B_u pairing state has point nodes on the k_z axis. The A_u pairing state may appear to be gapped since the staggered s-wave pairing [$\psi_{A_u}(\boldsymbol{k}) = a_4$] remains finite in the whole $\boldsymbol{k}$ space, but we will see that also the A_u pairing state can have point nodes on the k_z axis. For the E_u pairing state, the gap function is

$$\boldsymbol{d}_{E_u^{1,2}}(\boldsymbol{k}) = c_1(k_x \pm ik_y)\hat{\boldsymbol{z}} + c_2k_z(\hat{\boldsymbol{x}} \pm i\hat{\boldsymbol{y}}), \quad (7)$$

$$\psi_{E_u^{1,2}}(\boldsymbol{k}) = c_3(k_xk_z \pm ik_yk_z), \quad (8)$$

where the upper (lower) sign corresponds to the E_u^1 (E_u^2) state. Note that the magnetic field lifts the degeneracy of the E_u states. Under the high magnetic field along the c axis, the d vector parallel to the magnetic field ($\hat{z}$ component) is suppressed. In such a case, we expect a (pseudo) line node on the $k_z = 0$ plane.

Recently, it has been shown that the superconducting gap structures at given high-symmetry points in $\boldsymbol{k}$ space are precisely predicted by the topological classification [71–75], in which the gapless points are characterized by topological invariants. Especially, gap nodes protected by the nonsymmorphic space group symmetry and the total angular momentum of electrons are successfully found, consistent with previous group theoretical classifications [76–82]. Here, we classify the gap structure on the three different lines: (i) $k_x + k_y = 0$ lines with $k_z = 0$ and π, and the (ii) $k_x = k_y = 0$ line (k_z axis). The method of classification is given in the Supplemental Material [60].

Summary of classification of gap nodes is shown in Table III. For case (i), the A_u IR in the C_{2h} point group corresponds to the PDW state of A_u and B_u representations in C_{4h}. The classification with index 0 ($\mathbb{Z}$) indicates that the gap opens (closes) by the superconducting pair wave function when FSs in the normal state exist on the lines. In Table IV we summarize the excitation nodes for each pairing symmetry and FSs. For example, the A_u pairing state has a point node on the k_z axis for $U \leqslant 4$ eV (we again assumed the high magnetic field), while it is fully gapped for $U \geqslant 5$ eV. Table III is consistent with the result in Ref. [75].

TABLE IV. Excitation nodes and topological indices for odd-parity pairing states. A node of the superconducting gap appears on the k_z axis when FSs intersects the axis: $U \leqslant 4$ eV with the high magnetic field, while gapped otherwise.

	$k_x + k_y = 0$ lines	k_z axis	Topological index
A_u	gap	node/gap	$(\nu_{k_z}^{\mathfrak{g}^+}, \nu_{k_z}^{\mathfrak{g}^-}, C_{k_z})$
B_u	gap	node/gap	$(\nu_{k_z}^{\mathfrak{g}^+}, \nu_{k_z}^{\mathfrak{g}^-}, C_{k_z})$
E_u^1	node	node/gap	C_{k_z}
E_u^2	node	gap	C_{k_z}

Our analysis is based on the symmetry, and then it is assumed that the time-reversal symmetry is entirely broken. It corresponds to the situation that the magnetic field is sufficiently strong, and the d-vector parallel to the magnetic field is completely suppressed. For the $E_u^{1,2}$ states, we expect a line node on the $k_z = 0$ plane from Eq. (8), consistent with the nodes along the $k_x + k_y = 0$ lines. Although the topological classification does not give us any information on off-axis $\boldsymbol{k}$ points, the node on the $k_x + k_y = 0$ line should be interpreted as a part of the line node on the $k_z = 0$ plane.

It should be noticed that the TCSC discussed in Sec. II B is stable against excitation nodes. The 1D topological invariants on the $k_x + k_y = 0$ lines are well defined in any values of U, because the superconducting gap opens on these lines in the A_u and B_u superconducting states expected in $CeRh_2As_2$ at high magnetic fields. The corresponding Majorana surface states appear at the $(\bar{1}10)$ surface preserving the glide symmetry when the topological invariants in Tables I and II are nontrivial.

III. SUMMARY

In this Letter we have investigated the electronic state in $CeRh_2As_2$ by the DFT + U method and shown how the electron correlation changes the band structure, Fermi surface, and topological properties of superconductivity. A strong hybridization between Rh and Ce atoms at the Van Hove singularity and heavy electron pockets near the Brillouin zone corner are highlighted. The evolution of the Fermi surface as a function of U revealed a crossover from a 3D electron system to a quasi-2D one. A weak interlayer coupling favoring the 2D electronic structure and FSs near the zone corner of nonsymmorphic crystals are favorable features for the two superconducting phases with even and odd parity [3,16,22]. Thus, the correlation-induced FS evolution supports the PDW scenario for $CeRh_2As_2$.

The similarities of $CeRh_2As_2$ and iron-based superconductors were discussed. The hole pockets at the zone center

and the electron pockets at the zone corner are similar to the iron-based superconductors. While the nesting vector for the magnetic and quadrupole orders has been discussed [6,9], we expect the finite $\boldsymbol{q}$ nesting vector from our results: it would be $\boldsymbol{q} = (\pi, \pi, 0)$ if the electron correlation is strong enough.

The topological $\mathbb{Z}_2$ invariants for TCSC are evaluated from the Fermi surface formula, and the odd-parity superconducting states in the A_u and B_u representations are identified as the TCSC unless U is significantly large. Superconducting gap structures under the magnetic field are predicted by classification of symmetry and topology. The superconducting gap protecting the $\mathbb{Z}_2$ invariants are found to be robust, and Majorana surface states appear at the $(\bar{1}10)$ surface, preserving the glide symmetry. Because the high-field superconducting phase of $CeRh_2As_2$ is expected to be of the A_u or B_u representation, TCSC is predicted for a wide range of the parameter U. Although the band dispersion along the high symmetry line agrees with the ARPES experiment [58], the presence or absence of a small FS has not been investigated experimentally. Our calculations enable us to determine the topology in the PDW state from the normal electronic band structure, and thus, the observation of whole FSs is desirable for experimental verification.

In this Letter, we have ignored the effects of normal state order on superconductivity. This assumption is supported by the decoupling of the PDW state from the quadrupole order [8] and the magnetic order [5]. Because the normal state order is suppressed in the PDW state at high magnetic fields or pressures, our treatment is justified there. Even when the glide symmetry is broken by the quadrupole order in the coexisting region, a surface state reminiscent of the Majorana fermion is expected to appear.

ACKNOWLEDGMENTS

We appreciate helpful discussions with Y. Huang, B. Lv, X. Chen, E. Hassinger, K. Ishida, and M.H. Fischer. This work was supported by JSPS KAKENHI (Grants No. JP21K18145, No. JP22H04933, No. JP22H01181, No. JP22KJ1716, No. JP23K17353, No. JP24K21530, and No. JP24H00007) by the Swiss National Science Foundation (SNSF) Division II (No. 184739).

[1] S. Khim, J. F. Landaeta, J. Banda, N. Bannor, M. Brando, P. M. R. Brydon, D. Hafner, R. Küchler, R. Cardoso-Gil, U. Stockert, A. P. Mackenzie, D. F. Agterberg, C. Geibel, and E. Hassinger, Field-induced transition within the superconducting state of $CeRh_2As_2$, Science **373**, 1012 (2021).

[2] J. F. Landaeta, P. Khanenko, D. C. Cavanagh, C. Geibel, S. Khim, S. Mishra, I. Sheikin, P. M. R. Brydon, D. F. Agterberg, M. Brando, and E. Hassinger, Field-angle dependence reveals odd-parity superconductivity in $CeRh_2As_2$, Phys. Rev. X **12**, 031001 (2022).

[3] T. Yoshida, M. Sigrist, and Y. Yanase, Pair-density wave states through spin-orbit coupling in multilayer superconductors, Phys. Rev. B **86**, 134514 (2012).

[4] M. H. Fischer, M. Sigrist, D. F. Agterberg, and Y. Yanase, Superconductivity and local inversion-symmetry breaking, Annu. Rev. Condens. Matter Phys. **14**, 153 (2023).

[5] S. Ogata, S. Kitagawa, K. Kinjo, K. Ishida, M. Brando, E. Hassinger, C. Geibel, and S. Khim, Parity transition of spin-singlet superconductivity using sublattice degrees of freedom, Phys. Rev. Lett. **130**, 166001 (2023).

[6] D. Hafner, P. Khanenko, E.-O. Eljaouhari, R. Küchler, J. Banda, N. Bannor, T. Lühmann, J. F. Landaeta, S. Mishra, I. Sheikin, E. Hassinger, S. Khim, C. Geibel, G. Zwicknagl, and M. Brando, Possible quadrupole density wave in the superconducting Kondo lattice $CeRh_2As_2$, Phys. Rev. X **12**, 011023 (2022).

[7] S. Mishra, Y. Liu, E. D. Bauer, F. Ronning, and S. M. Thomas, Anisotropic magnetotransport properties of the heavy-fermion superconductor $CeRh_2As_2$, Phys. Rev. B **106**, L140502 (2022).

[8] K. Semeniuk, D. Hafner, P. Khanenko, T. Lühmann, J. Banda, J. F. Landaeta, C. Geibel, S. Khim, E. Hassinger, and M. Brando, Decoupling multiphase superconductivity from normal state ordering in $CeRh_2As_2$, Phys. Rev. B **107**, L220504 (2023).

[9] M. Kibune, S. Kitagawa, K. Kinjo, S. Ogata, M. Manago, T. Taniguchi, K. Ishida, M. Brando, E. Hassinger, H. Rosner, C. Geibel, and S. Khim, Observation of antiferromagnetic order as odd-parity multipoles inside the superconducting phase in $CeRh_2As_2$, Phys. Rev. Lett. **128**, 057002 (2022).

[10] S. Kitagawa, M. Kibune, K. Kinjo, M. Manago, T. Taniguchi, K. Ishida, M. Brando, E. Hassinger, C. Geibel, and S. Khim, Two-dimensional xy-type magnetic properties of locally noncentrosymmetric superconductor $CeRh_2As_2$, J. Phys. Soc. Jpn. **91**, 043702 (2022).

[11] E. G. Schertenleib, M. H. Fischer, and M. Sigrist, Unusual H-T phase diagram of $CeRh_2As_2$: The role of staggered noncentrosymmetricity, Phys. Rev. Res. **3**, 023179 (2021).

[12] A. Skurativska, M. Sigrist, and M. H. Fischer, Spin response and topology of a staggered-Rashba superconductor, Phys. Rev. Res. **3**, 033133 (2021).

[13] K. Nogaki, A. Daido, J. Ishizuka, and Y. Yanase, Topological crystalline superconductivity in locally noncentrosymmetric $CeRh_2As_2$, Phys. Rev. Res. **3**, L032071 (2021).

[14] D. Möckli and A. Ramires, Superconductivity in disordered locally noncentrosymmetric materials: An application to $CeRh_2As_2$, Phys. Rev. B **104**, 134517 (2021).

[15] A. Ptok, K. J. Kapcia, P. T. Jochym, J. Łażewski, A. M. Oleś, and P. Piekarz, Electronic and dynamical properties of $CeRh_2As_2$: Role of Rh_2As_2 layers and expected orbital order, Phys. Rev. B **104**, L041109 (2021).

[16] D. C. Cavanagh, T. Shishidou, M. Weinert, P. M. R. Brydon, and D. F. Agterberg, Nonsymmorphic symmetry and field-driven odd-parity pairing in $CeRh_2As_2$, Phys. Rev. B **105**, L020505 (2022).

[17] K. Nogaki and Y. Yanase, Even-odd parity transition in strongly correlated locally noncentrosymmetric superconductors: Application to $CeRh_2As_2$, Phys. Rev. B **106**, L100504 (2022).

[18] T. Hazra and P. Coleman, Triplet pairing mechanisms from Hund's-Kondo models: Applications to UTe_2 and $CeRh_2As_2$, Phys. Rev. Lett. **130**, 136002 (2023).

[19] K. Machida, Violation of Pauli-Clogston limit in the heavy-fermion superconductor $CeRh_2As_2$: Duality of itinerant and localized $4f$ electrons, Phys. Rev. B **106**, 184509 (2022).

[20] S. Onishi, U. Stockert, S. Khim, J. Banda, M. Brando, and E. Hassinger, Low-temperature thermal conductivity of the two-phase superconductor $CeRh_2As_2$, Front. Electron. Mater. **2**, 880579 (2022).

[21] A. Amin, H. Wu, T. Shishidou, and D. F. Agterberg, Kramers' degenerate magnetism and superconductivity, Phys. Rev. B **109**, 024502 (2024).

[22] S. Sumita and Y. Yanase, Superconductivity in magnetic multipole states, Phys. Rev. B **93**, 224507 (2016).

[23] S.-i. Kimura, J. Sichelschmidt, and S. Khim, Optical study of the electronic structure of locally noncentrosymmetric $CeRh_2As_2$, Phys. Rev. B **104**, 245116 (2021).

[24] X.-L. Qi and S.-C. Zhang, Topological insulators and superconductors, Rev. Mod. Phys. **83**, 1057 (2011).

[25] M. Sato and S. Fujimoto, Majorana fermions and topology in superconductors, J. Phys. Soc. Jpn. **85**, 072001 (2016).

[26] M. Sato and Y. Ando, Topological superconductors: A review, Rep. Prog. Phys. **80**, 076501 (2017).

[27] A. P. Schnyder, S. Ryu, A. Furusaki, and A. W. W. Ludwig, Classification of topological insulators and superconductors in three spatial dimensions, Phys. Rev. B **78**, 195125 (2008).

[28] A. Kitaev, Periodic table for topological insulators and superconductors, AIP Conf. Proc. **1134**, 22 (2009).

[29] S. Ryu, A. P. Schnyder, A. Furusaki, and A. W. W. Ludwig, Topological insulators and superconductors: Tenfold way and dimensional hierarchy, New J. Phys. **12**, 065010 (2010).

[30] L. Fu, Topological crystalline insulators, Phys. Rev. Lett. **106**, 106802 (2011).

[31] F. Zhang, C. L. Kane, and E. J. Mele, Topological mirror superconductivity, Phys. Rev. Lett. **111**, 056403 (2013).

[32] C.-K. Chiu, H. Yao, and S. Ryu, Classification of topological insulators and superconductors in the presence of reflection symmetry, Phys. Rev. B **88**, 075142 (2013).

[33] T. Morimoto and A. Furusaki, Topological classification with additional symmetries from clifford algebras, Phys. Rev. B **88**, 125129 (2013).

[34] K. Shiozaki and M. Sato, Topology of crystalline insulators and superconductors, Phys. Rev. B **90**, 165114 (2014).

[35] C.-K. Chiu and A. P. Schnyder, Classification of reflection-symmetry-protected topological semimetals and nodal superconductors, Phys. Rev. B **90**, 205136 (2014).

[36] Y. Ueno, A. Yamakage, Y. Tanaka, and M. Sato, Symmetry-protected Majorana fermions in topological crystalline superconductors: Theory and application to Sr_2RuO_4, Phys. Rev. Lett. **111**, 087002 (2013).

[37] Y. Tsutsumi, M. Ishikawa, T. Kawakami, T. Mizushima, M. Sato, M. Ichioka, and K. Machida, UPt_3 as a topological crystalline superconductor, J. Phys. Soc. Jpn. **82**, 113707 (2013).

[38] T. Yoshida, M. Sigrist, and Y. Yanase, Topological crystalline superconductivity in locally noncentrosymmetric multilayer superconductors, Phys. Rev. Lett. **115**, 027001 (2015).

[39] C. Fang and L. Fu, New classes of three-dimensional topological crystalline insulators: Nonsymmorphic and magnetic, Phys. Rev. B **91**, 161105(R) (2015).

[40] K. Shiozaki, M. Sato, and K. Gomi, Z_2 topology in nonsymmorphic crystalline insulators: Möbius twist in surface states, Phys. Rev. B **91**, 155120 (2015).

[41] K. Shiozaki, M. Sato, and K. Gomi, Topology of nonsymmorphic crystalline insulators and superconductors, Phys. Rev. B **93**, 195413 (2016).

[42] H. Shapourian, Y. Wang, and S. Ryu, Topological crystalline superconductivity and second-order topological superconductivity in nodal-loop materials, Phys. Rev. B **97**, 094508 (2018).

[43] Y. Yanase and K. Shiozaki, Möbius topological superconductivity in UPt_3, Phys. Rev. B **95**, 224514 (2017).

[44] A. Daido, T. Yoshida, and Y. Yanase, $\mathbb{Z}_4$ topological superconductivity in UCoGe, Phys. Rev. Lett. **122**, 227001 (2019).

[45] S. Ono, Y. Yanase, and H. Watanabe, Symmetry indicators for topological superconductors, Phys. Rev. Res. **1**, 013012 (2019).

[46] S. Ono, H. C. Po, and H. Watanabe, Refined symmetry indicators for topological superconductors in all space groups, Sci. Adv. **6**, eaaz8367 (2020).

[47] S. Ono, H. C. Po, and K. Shiozaki, $\mathbb{z}_2$-enriched symmetry indicators for topological superconductors in the 1651 magnetic space groups, Phys. Rev. Res. **3**, 023086(R) (2021).

[48] A. Skurativska, T. Neupert, and M. H. Fischer, Atomic limit and inversion-symmetry indicators for topological superconductors, Phys. Rev. Res. **2**, 013064 (2020).

[49] M. Geier, P. W. Brouwer, and L. Trifunovic, Symmetry-based indicators for topological Bogoliubov–de Gennes hamiltonians, Phys. Rev. B **101**, 245128 (2020).

[50] K. Shiozaki, Variants of the symmetry-based indicator, arXiv:1907.13632.

[51] J. Ahn and B.-J. Yang, Higher-order topological superconductivity of spin-polarized fermions, Phys. Rev. Res. **2**, 012060(R) (2020).

[52] K. Haule, C.-H. Yee, and K. Kim, Dynamical mean-field theory within the full-potential methods: Electronic structure of $CeIrIn_5$, $CeCoIn_5$, and $CeRhIn_5$, Phys. Rev. B **81**, 195107 (2010).

[53] T. Nomoto and H. Ikeda, Fermi surface evolution and d-wave superconductivity in $CeCoIn_5$: Analysis based on LDA + DMFT method, Phys. Rev. B **90**, 125147 (2014).

[54] H. C. Choi, B. I. Min, J. H. Shim, K. Haule, and G. Kotliar, Temperature-dependent Fermi surface evolution in heavy fermion $CeIrIn_5$, Phys. Rev. Lett. **108**, 016402 (2012).

[55] H. Ikeda, M.-T. Suzuki, and R. Arita, Emergent loop-nodal $s_{\pm}$-wave superconductivity in $CeCu_2Si_2$: Similarities to the iron-based superconductors, Phys. Rev. Lett. **114**, 147003 (2015).

[56] J. Ishizuka, S. Sumita, A. Daido, and Y. Yanase, Insulator-metal transition and topological superconductivity in UTe_2 from a first-principles calculation, Phys. Rev. Lett. **123**, 217001 (2019).

[57] Y. Xu, Y. Sheng, and Y.-f. Yang, Quasi-two-dimensional Fermi surfaces and unitary spin-triplet pairing in the heavy fermion superconductor UTe_2, Phys. Rev. Lett. **123**, 217002 (2019).

[58] X. Chen, L. Wang, J. Ishizuka, R. Zhang, K. Nogaki, Y. Cheng, F. Yang, Z. Chen, F. Zhu, Z. Liu, J. Mei, Y. Yanase, B. Lv, and Y. Huang, Coexistence of near-E_F flat band and van Hove singularity in a two-phase superconductor, Phys. Rev. X **14**, 021048 (2024).

[59] Y. Wu, Y. Zhang, S. Ju, Y. Hu, Y. Huang, Y. Zhang, H. Zhang, H. Zheng, G. Yang, E.-O. Eljaouhari, B. Song, N. C. Plumb, F. Steglich, M. Shi, G. Zwicknagl, C. Cao, H. Yuan, and Y. Liu, Fermi surface nesting with heavy quasiparticles in the locally noncentrosymmetric superconductor $CeRh_2As_2$, Chinese Phys. Lett. **41**, 097403 (2024).

[60] See Supplemental Material at http://link.aps.org/supplemental/10.1103/PhysRevB.110.L140505 for details, which includes Refs. [83–92].

[61] I. I. Mazin, D. J. Singh, M. D. Johannes, and M. H. Du, Unconventional superconductivity with a sign reversal in the order parameter of $LaFeAsO_{1-x}F_x$, Phys. Rev. Lett. **101**, 057003 (2008).

[62] K. Kuroki, S. Onari, R. Arita, H. Usui, Y. Tanaka, H. Kontani, and H. Aoki, Unconventional pairing originating from the disconnected Fermi surfaces of superconducting $LaFeAsO_{1-x}F_x$, Phys. Rev. Lett. **101**, 087004 (2008).

[63] R. M. Fernandes, L. H. VanBebber, S. Bhattacharya, P. Chandra, V. Keppens, D. Mandrus, M. A. McGuire, B. C. Sales, A. S. Sefat, and J. Schmalian, Effects of nematic fluctuations on the elastic properties of iron arsenide superconductors, Phys. Rev. Lett. **105**, 157003 (2010).

[64] Y. Yanagi, Y. Yamakawa, N. Adachi, and Y. Ōno, Orbital order, structural transition, and superconductivity in iron pnictides, J. Phys. Soc. Jpn. **79**, 123707 (2010).

[65] H. Kontani, T. Saito, and S. Onari, Origin of orthorhombic transition, magnetic transition, and shear-modulus softening in iron pnictide superconductors: Analysis based on the orbital fluctuations theory, Phys. Rev. B **84**, 024528 (2011).

[66] S. Onari and H. Kontani, Self-consistent vertex correction analysis for iron-based superconductors: Mechanism of Coulomb interaction-driven orbital fluctuations, Phys. Rev. Lett. **109**, 137001 (2012).

[67] L. Fu and E. Berg, Odd-parity topological superconductors: Theory and application to $Cu_xBi_2Se_3$, Phys. Rev. Lett. **105**, 097001 (2010).

[68] M. Sato, Topological odd-parity superconductors, Phys. Rev. B **81**, 220504(R) (2010).

[69] Y. Yanase, Nonsymmorphic Weyl superconductivity in UPt_3 based on E_{2u} representation, Phys. Rev. B **94**, 174502 (2016).

[70] M. Sigrist and K. Ueda, Phenomenological theory of unconventional superconductivity, Rev. Mod. Phys. **63**, 239 (1991).

[71] S. Kobayashi, K. Shiozaki, Y. Tanaka, and M. Sato, Topological Blount's theorem of odd-parity superconductors, Phys. Rev. B **90**, 024516 (2014).

[72] S. Kobayashi, Y. Yanase, and M. Sato, Topologically stable gapless phases in nonsymmorphic superconductors, Phys. Rev. B **94**, 134512 (2016).

[73] S. Kobayashi, S. Sumita, Y. Yanase, and M. Sato, Symmetry-protected line nodes and Majorana flat bands in nodal crystalline superconductors, Phys. Rev. B **97**, 180504(R) (2018).

[74] S. Sumita, T. Nomoto, K. Shiozaki, and Y. Yanase, Classification of topological crystalline superconducting nodes on high-symmetry lines: Point nodes, line nodes, and Bogoliubov Fermi surfaces, Phys. Rev. B **99**, 134513 (2019).

[75] S. Ono and K. Shiozaki, Symmetry-based approach to superconducting nodes: Unification of compatibility conditions and gapless point classifications, Phys. Rev. X **12**, 011021 (2022).

[76] V. G. Yarzhemsky and E. N. Murav'ev, Space group approach to the wavefunction of a cooper pair, J. Phys.: Condens. Matter **4**, 3525 (1992).

[77] M. R. Norman, Odd parity and line nodes in heavy-fermion superconductors, Phys. Rev. B **52**, 15093 (1995).

[78] T. Micklitz and M. R. Norman, Odd parity and line nodes in nonsymmorphic superconductors, Phys. Rev. B **80**, 100506(R) (2009).

[79] T. Nomoto and H. Ikeda, Symmetry-protected line nodes in non-symmorphic magnetic space groups: Applications to UCoGe and UPd_2Al_3, J. Phys. Soc. Jpn. **86**, 023703 (2017).

[80] T. Micklitz and M. R. Norman, Symmetry-enforced line nodes in unconventional superconductors, Phys. Rev. Lett. **118**, 207001 (2017).

[81] S. Sumita, T. Nomoto, and Y. Yanase, Multipole superconductivity in nonsymmorphic Sr_2IrO_4, Phys. Rev. Lett. **119**, 027001 (2017).

[82] S. Sumita and Y. Yanase, Unconventional superconducting gap structure protected by space group symmetry, Phys. Rev. B **97**, 134512 (2018).

[83] P. Blaha, K. Schwarz, G. K. H. Madsen, D. Kvasnicka, J. Luitz, R. Laskowski, F. Tran, and L. D. Marks, *WIEN2k, An Augmented Plane Wave + Local Orbitals Program for Calculating Crystal Properties* (Karlheinz Schwarz, Techn. Universität Wien, Austria, 2018).

[84] M. T. Czyżyk and G. A. Sawatzky, Local-density functional and on-site correlations: The electronic structure of La_2CuO_4 and $LaCuO_3$, Phys. Rev. B **49**, 14211 (1994).

[85] E. P. Wigner, *Group Theory and Its Application to the Quantum Mechanics of Atomic Spectra* (Academic Press, New York, 1959).

[86] C. Herring, Effect of time-reversal symmetry on energy bands of crystals, Phys. Rev. **52**, 361 (1937).

[87] T. Inui, Y. Tanabe, and Y. Onodera, *Group Theory and Its Applications in Physics*, Springer Series in Solid-State Sciences, Vol. 78 (Springer-Verlag Berlin Heidelberg, Berlin, Heidelberg, 1990).

[88] C. J. Bradley and A. P. Cracknell, *The Mathematical Theory of Symmetry in Solids* (Oxford University Press, Oxford, 1972).

[89] K. Shiozaki, M. Sato, and K. Gomi, Atiyah-hirzebruch spectral sequence in band topology: General formalism and topological invariants for 230 space groups, Phys. Rev. B **106**, 165103 (2022).

[90] J. Kuneš, R. Arita, P. Wissgott, A. Toschi, H. Ikeda, and K. Held, Wien2wannier: From linearized augmented plane waves to maximally localized wannier functions, Comput. Phys. Commun. **181**, 1888 (2010).

[91] G. Pizzi, V. Vitale, R. Arita, S. Blügel, F. Freimuth, G. Géranton, M. Gibertini, D. Gresch, C. Johnson, T. Koretsune, J. Ibañez-Azpiroz, H. Lee, J.-M. Lihm, D. Marchand, A. Marrazzo, Y. Mokrousov, J. I. Mustafa, Y. Nohara, Y. Nomura, L. Paulatto *et al.*, Wannier90 as a community code: New features and applications, J. Phys.: Condens. Matter **32**, 165902 (2020).

[92] G.-X. Zhi, C. Xu, S.-Q. Wu, F. Ning, and C. Cao, Wannsymm: A symmetry analysis code for wannier orbitals, Comput. Phys. Commun. **271**, 108196 (2022).